

Cite this: *J. Mater. Chem. C*, 2021,  
9, 9465

# Elastic orange emissive single crystals of 1,3-diamino-2,4,5,6-tetrabromobenzene as flexible optical waveguides†

Venkatesh Gude,<sup>a</sup> Priyanka S. Choubey,<sup>b</sup> Susobhan Das,<sup>c</sup>  
Shivakiran Bhaktha B. N.,<sup>bd</sup> C. Malla Reddy<sup>id</sup>\*<sup>c</sup> and Kumar Biradha<sup>id</sup>\*<sup>a</sup>

Single crystals of monoaromatic compounds exhibiting both mechanical softness and optical properties have attracted significant scientific interest in recent years, but they are very scarce. Herein, single crystals of 1,3-diamino-2,4,5,6-tetrabromobenzene (compound **1**) were shown to exhibit excellent and unexpected elastic behaviour upon mechanical deformation. The crystal structure analysis of **1** illustrates the intermolecular interactions (Br...Br, N...Br and N-H...Br) that are responsible for such flexible behaviour. Furthermore, the elastic modulus of crystals of **1** is found to be around 12 GPa, which was determined through nanoindentation experiments on the bendable major (100) face. In addition, interestingly, compound **1** was also found to exhibit optical properties in the longer wavelength region (orange emission) both in the solid and solution states despite not having any significant extended conjugation. To rationalize the experimentally observed optical behaviour, time-dependent density functional theory (TDDFT) calculations have been performed. The potential use of single crystals of **1** has been tested in optical waveguide applications. The present work demonstrates the significance of soft interaction guided packing in the origin of both mechanical and optical properties of organic single crystals.

Received 21st April 2021,  
Accepted 4th June 2021

DOI: 10.1039/d1tc01841h

rsc.li/materials-c

## Introduction

The mechanical properties such as plasticity and elasticity of an organic single crystal are a manifestation of non-covalent interaction guided molecular packing.<sup>1–3</sup> Most of the crystals undergo brittle fracture when an external load is applied. Therefore, the search for crystals with compliant mechanical properties is extremely important in order to develop flexible device technologies.<sup>4,5</sup> Both qualitative and quantitative studies which are performed on flexible crystals have incredible potential in developing pharmaceutical solids.<sup>6</sup> Furthermore, single crystals of organic compounds possessing a combination of fluorescence and flexible mechanical properties are highly

interesting owing to their significant impact in developing flexible optical waveguides<sup>7–10</sup>/electronics<sup>11–18</sup> and mechano-photonic applications.<sup>19–23</sup>

At the fundamental level, the molecular packing features which are essential for single crystals to exhibit plasticity, elasticity and brittle behaviour are well documented, yet design principles are still evolving.<sup>2</sup> In principle, the significant degree of strength of interaction gradients in orthogonal directions of a crystal leads to an irreversible migration (plastic behaviour) of molecules along the slip planes when the load is applied in a perpendicular direction.<sup>24</sup> Similarly, crystals with soft interactions generally with an interlocked structure lead to a reversible migration (elastic behaviour) of molecules along the outer and inner arcs when subjected to loading-unloading cycles.<sup>25–27</sup> Furthermore, upon mechanical deformation, the fracture of a crystal (brittle behaviour) is observed when there is isotropic strength of interactions in all directions and in the absence of facile slip planes.<sup>2</sup>

Recently, the optical and mechanical properties of monoaromatic compounds have gained significant scientific interest due to their potential application in flexible optical waveguides.<sup>28,29</sup> It is important to note that achieving both optical and flexible mechanical properties in single crystals of monoaromatic compounds is rare and challenging,<sup>30</sup> and our work on 1,3-diamino-2,4,5,6-tetrabromobenzene (compound **1**, Scheme 1) aims to fill

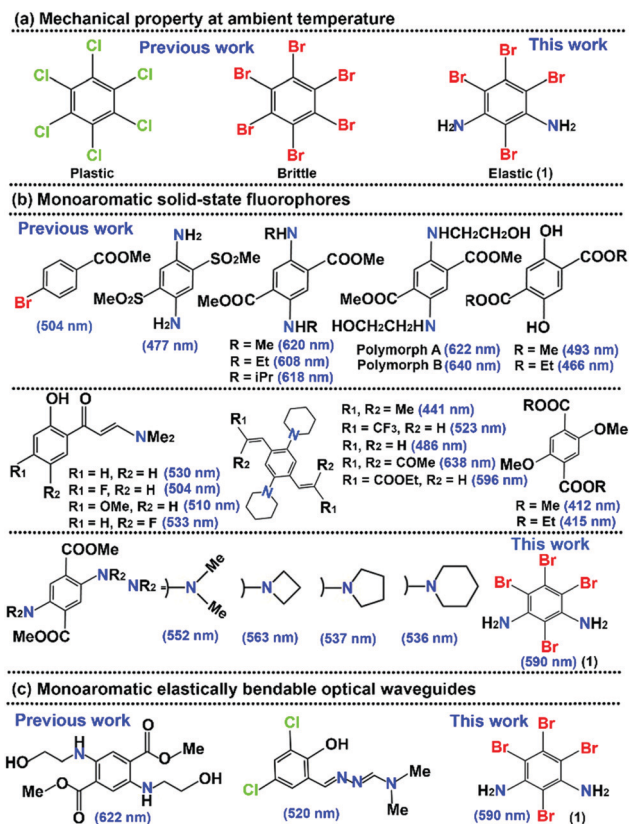
<sup>a</sup> Department of Chemistry, Indian Institute of Technology-Kharagpur, Kharagpur, West Bengal, 721302, India. E-mail: kbiradha@chem.iitkgp.ac.in

<sup>b</sup> School of Nano-Science and Technology, Indian Institute of Technology-Kharagpur, Kharagpur, West Bengal, 721302, India

<sup>c</sup> Department of Chemical Sciences, Indian Institute of Science Education and Research Kolkata, Nadia, West Bengal, 741246, India.  
E-mail: cmallareddy@gmail.com

<sup>d</sup> Department of Physics, Indian Institute of Technology-Kharagpur, Kharagpur, West Bengal, 721302, India

† Electronic supplementary information (ESI) available: Details of synthesis, <sup>1</sup>HNMR results, optical waveguide experiments, elastic strain, crystallographic parameters and computational results. CCDC 2077700. For ESI and crystallographic data in CIF or other electronic format see DOI: 10.1039/d1tc01841h



Scheme 1 Molecular structures representing the (a) mechanical (b) emissive and (c) flexible optical waveguide behaviour of monoaromatic compounds.

this gap. Furthermore, our focus in the present work is restricted to monoaromatic compounds with mechanical softness.<sup>31,32</sup> A few compounds which are structurally relevant to the present work are shown in Scheme 1a. For instance, hexachlorobenzene is known to bend plastically at room temperature while hexabromobenzene (isostructural) is brittle but bends at a higher temperature.<sup>31,33</sup> Interestingly, the single crystals of compound **1** are found to exhibit remarkable elastic flexibility at room temperature. Note that the difference between compound **1** and hexabromobenzene is that the two amino groups in the former are at the *meta* position instead of Br atoms in the latter. The amino groups in compound **1** are expected to form strong hydrogen and halogen bonds (e.g., N–H...N, N...Br) compared to hexabromobenzene which solely exhibits Br...Br interactions (moderate strength). In order to understand the structure and mechanical property correlation, a detailed study was carried out on single crystals of **1**.

Furthermore, there are various types of fluorophores which could exhibit superior optical properties in the solid-state and are comparable to  $\pi$ -conjugated materials.<sup>34–41</sup> To the best of our knowledge these monoaromatic fluorophores exhibit an emission maximum (Scheme 1b) which covers almost the entire visible wavelength (blue to red region) indicating their significance for practical applications.<sup>42–44</sup> It is important to note that monoaromatic compounds displaying an orange emission are very rare. None of the reported emitters<sup>34–44</sup> shown in Scheme 1b exhibit mechanical flexibility in the

crystalline state with the exception of one example that also shows polymorphism.<sup>28</sup> Zhang and his co-workers contributed extensively to obtaining single crystals which can exhibit both efficient optical and elastic properties. Furthermore, they have tested the potential of crystals in flexible optical waveguide applications.<sup>28,29</sup> To the best of our knowledge, there are two reports available on monoaromatic compounds which can act as elastically bendable optical waveguides (Scheme 1c).<sup>28,29</sup> Herein, we report the synthesis, and optical and mechanical (elastic) properties of single crystals of compound **1** and their application in flexible optical waveguides. It is important to note that the molecular structure of **1** is significantly different from that of the two reported compounds, in which the phenyl ring is in extended conjugation with other functional groups.

## Results and discussion

Compound **1** was synthesized and characterized as detailed in the ESI.† The recrystallized compound **1** was used to obtain acicular single crystals by slow evaporation of the mixture of solvents (THF & MeOH).

The mechanical properties of the single crystals of **1** have been tested qualitatively by using a pair of forceps and metallic needle at ambient temperature. When the (100) plane was supported by forceps and the mechanical force was applied from the opposite side (–100), the needle shaped crystal was bent into a semicircular shape (Fig. 1a–d). The crystal can be repeatedly bent into an arc shape without breaking (Video S1, ESI†). Upon exceeding a certain threshold of force, the crystal was fragmented into pieces (Fig. 1e). Interestingly, when a fragmented piece was subjected to mechanical stress again, it

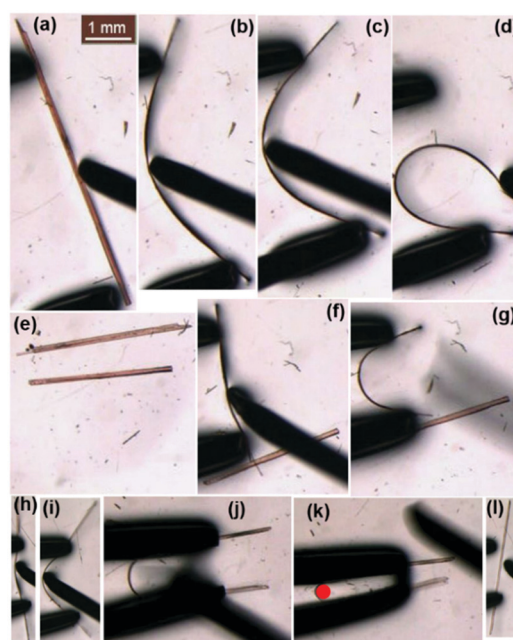


Fig. 1 Optical microscopy images demonstrating the qualitative elastic bending behaviour of single crystals of **1** when subjected to mechanical stress.

showed the original elastic nature (Fig. 1f, g and Video S1, ESI†). Furthermore, in order to calculate the maximum elastic strain using the Euler–Bernoulli beam-bending theory,<sup>45</sup> the crystal of **1** was subjected to mechanical stress without crossing the elastic limit (Fig. 1h–j) so as to form an arc or a semicircle (Fig. 1k and Video S2, ESI†).

The calculated elastic strain was found to be over ~15% (Fig. S1, ESI†). This value is comparable to the previously reported highest elastic strain bearing yellow needles of ROY<sup>46</sup> (~14.6%) and crystal fibers<sup>47</sup> (~14.28%), indicating the exceptional ability of the crystal to dissipate mechanical stress (Fig. 1k and l). However, after exceeding the stress beyond the elastic limit, the crystal undergoes brittle fracture without leaving any significant plastic deformation in the fragmented pieces (Video S2, ESI†). The pristine crystals and their fragmented pieces did not exhibit any noticeable plastic (permanent) deformation after several repeat loading–unloading cycles, indicating the usefulness of the elasticity.

In order to understand the molecular packing features that are responsible for the elastic behaviour of compound **1**, the single crystal X-ray diffraction (SCXRD) analysis was performed. Compound **1** crystallizes in the  $P2_1/c$  space group with one molecule in the asymmetric unit. The pertinent crystallographic parameters for compound **1** are given in Table S1 (ESI†). The experimental powder XRD pattern of compound **1** is found to be identical to its simulated XRD pattern (Fig. S2, ESI†), indicating the phase purity of **1**. The differential scanning calorimetry (DSC) thermogram also indicates no significant phase change prior to melting of **1** (Fig. S3, ESI†).

The computed electrostatic potential (ESP) coloured molecular van der Waals (vdW) surface map (Fig. 2a) indicates that there are three chemically different bromine atoms in compound **1**. The blue and red regions correspond to the negative and positive ESP surfaces. The strength of the  $\sigma$ -holes of Br atoms follows the decreasing order: Br-II (20.66 kcal mol<sup>-1</sup>) > Br-I (16.8 kcal mol<sup>-1</sup>) > Br-III (14.9 kcal mol<sup>-1</sup>).<sup>48,49</sup> The Br-II and Br-IV are chemically equivalent with the same strength of  $\sigma$ -holes. In the crystal structure, the molecules of **1** form dimers (Fig. 2b) *via* Br··Br (type-II) interactions (3.61 Å,  $\theta_1 = 170.1^\circ$ ,  $\theta_2 = 128.6^\circ$ ). These dimers are connected to each other through halogen bonds (N··Br, 3.33 Å) and N–H··Br (H··Br, 3.03 Å, 173.9°) hydrogen bonds to form an infinite 1D-chain. The adjacent 1D-chains are connected through Br··Br (3.66 Å,  $\theta_1 = \theta_2 = 146.9^\circ$ ) type-I interactions and N–H··N (H··N, 2.24 Å, 164.1°) hydrogen bonds to form a corrugated 2D-sheet in the *ac*-plane (Fig. 2b) which are  $\pi$ -stacked to form a crystal lattice. Overall, the non-covalent interactions between the molecules such as slipped  $\pi$ - $\pi$  stacking (3.59 Å) along [010], C–N··Br, N–H··Br along [100] and Br··Br along [001] create near isotropic and corrugated/interlocked packing patterns in mutually perpendicular directions (Fig. 2c).<sup>2,50</sup> In the structure analysis of **1**, among the four bromine atoms, three (II, III, and IV) are involved in type-II (less than 2 kcal mol<sup>-1</sup>; Fig. S4, ESI†)<sup>48,51</sup> and one (I) in type-I halogen–halogen interactions. Furthermore, when these crystals are subjected to mechanical stress in the (100) face, the type-II Br··Br interactions are

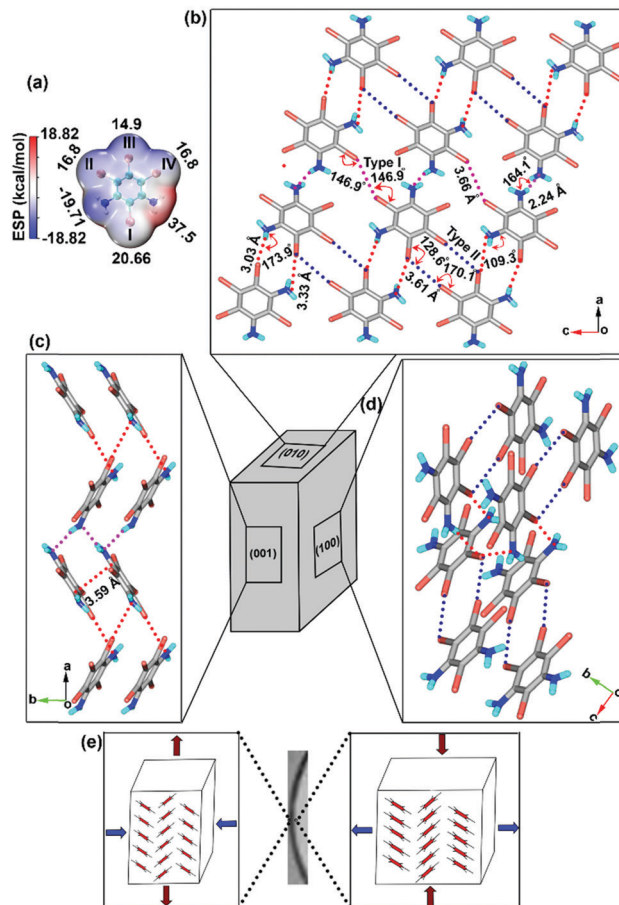


Fig. 2 (a) Computed ESP coloured molecular vdW surface map (iso value = 0.001) of compound **1**. Numerical numbers represent the energy in kcal mol<sup>-1</sup>. (b), (c) and (d) Crystal morphology with face indices and packing for down (010), up (001) and (100) faces, respectively. (e) Schematic representation of the changes in crystal packing along the outer (left) and inner (right) arcs upon deformation. For clarity, the substituents over the benzene are omitted.

expected to bear the strain to accommodate local molecular rotations (Fig. 2d).

We would like to note here that Br··Br interactions are known to provide such “structural buffering” during deformation.<sup>52</sup> In other words, they are soft enough to accommodate the mechanical strain during the flexure and act as restoring forces upon withdrawal of the load. As the plastic deformation in crystals of **1** was not observed, we suggest that the corrugated packing pattern with isotropic interactions does not favour the long-range molecular movement during deformation of the crystal, hence the crystals manifest the elastic properties and directly fracture at higher strains.<sup>2</sup> Therefore, it could be anticipated that the Br··Br interactions will experience the strain upon bending of the crystal. Furthermore, the length of elastic crystals increases in the outer arc (tensile stress) and decreases in the inner arc (compressive stress) upon bending.<sup>2,25,27</sup> Recently, Worthy *et al.* experimentally confirmed that during the course of elastic bending, the molecular rotations facilitate the compression along the interior of the arc with simultaneous expansion of the outer arc.<sup>26</sup> Therefore,

higher strain in the crystals is expected to cause not only splaying (rotations) of molecules but also change in molecular distances when compared to thermodynamic equilibrium positions at the centre of the crystal (Fig. 2e).<sup>19,26,27,53</sup>

The nanoindentation technique was employed in order to quantify the observed mechanical properties, namely elastic modulus ( $E$ ) and hardness ( $H$ ) of single crystals. The indentation experiments were performed on the bendable major face (100) of single crystals using a Berkovich indenter diamond tip.<sup>27,54</sup> During the experiments, a load ( $P$ ) of 6 mN is applied and the corresponding depth of penetration ( $h$ ) of the indenter is monitored. The absence of pop-in events on the loading part of the  $P$ - $h$  curve (Fig. 3a) indicates that a sudden elastic to plastic transition is not observed.<sup>6</sup> Furthermore, the smooth nature of the loading part of the  $P$ - $h$  curve and moderate depth recovery during unloading suggest that this crystal face is soft. This is reasonable as the indentation direction is parallel to the plane intersecting Br $\cdots$ Br interactions. The  $E$  and  $H$  values extracted from the indentation experiments are found to be  $12.3 \pm 0.3$  and  $0.48 \pm 0.01$  GPa, respectively. These values are comparable to some of the reported elastically bendable organic single crystals.<sup>55</sup> The *in situ* scanning probe images (Fig. 3b-d) of nanoindenter impressions describe the height profiles for the major face (100). No significant pile-up was observed surrounding the indent impression (Fig. 3c and d). The results for this face indicate its compressible nature which is consistent with its soft nature.

In order to investigate the optical properties, steady state diffuse reflectance spectra (DRS) and photoluminescence spectra (PLS) of compound **1** were recorded in the solid state (Fig. 4a). Compound **1** possesses two absorption bands with a maximum at 315 nm and a weak broad shoulder in the region of 400–600 nm. Similar absorption features (Fig. 4b) of **1** were noticed in hexane, dichloromethane (DCM) and MeOH. But,

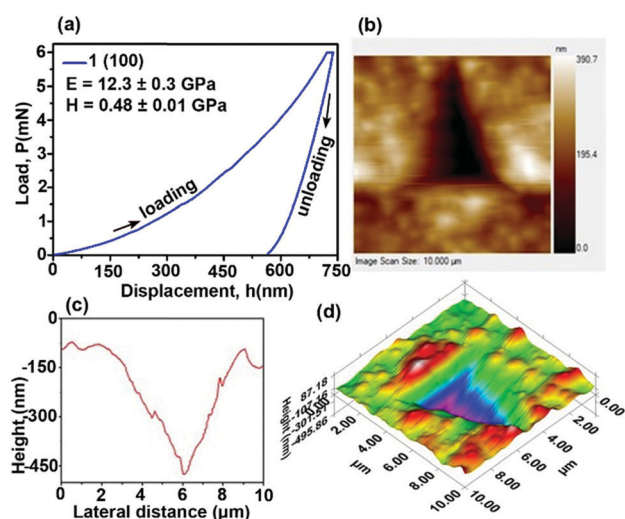


Fig. 3 Nanoindentation results. (a) The representative load–depth ( $P$ - $h$ ) curve obtained by indenting on the major (100) face. *In situ* scanning probe images of post-nanoindentation impressions. (b) 2D indent impression, (c) height profile and (d) their 3D projection.

the weak absorption band is broadened and the maximum is red-shifted when moving from non-polar to polar solvents (Fig. S5a, ESI†). To rationalize the experimental solid and solution absorption properties and to understand the nature of transitions, single point energy calculations were performed on ground state ( $S_0$ ) optimized geometry with the PBE/PBE functional<sup>56</sup> and double zeta valence plus polarization function (DZVP) basis set<sup>57,58</sup> using the TDDFT method.<sup>59</sup> All the calculations were performed using the Gaussian 09 package.<sup>60</sup>

The experimentally observed absorption maximum is significantly overlapped with the calculated absorption maximum (Fig. S6a-c, ESI†). Upon excitation at 480 nm both in solid and DCM, compound **1** exhibited orange emission with the maximum at 590 and 575 nm, respectively. Furthermore, these emission bands are extended into the red region till 700 nm (Fig. 4a and b), whereas, in MeOH the emission maximum is 40 nm red-shifted. This redshift of absorption and emission maximum in MeOH when compared to that in DCM is attributed to the solvent polarity effect. The recorded excitation spectra (Fig. S6d, ESI†) exhibit similar absorption features (peak positions) of compound **1**, indicating that no new excited species are formed during optical excitation. It is important to note that the origin of the orange emission of compound **1** is significantly different when compared with that of the recently reported monoaromatic fluorophore,<sup>29</sup> in which, the excited state intramolecular proton transfer (ESIPT) process is responsible for the observed green emission ( $\lambda_{\text{max}} = 520$  nm). Furthermore, upon careful observation of each monoaromatic chromophore structure reported so far (Scheme 1b and c),<sup>34-44</sup> it can be understood that the benzenoid ring is in conjugation with the substituted functional group such as carbonyl, sulphonyl, alkene, *etc.* However, in the present work, the benzenoid ring of compound **1** is not in conjugation with any substituted functional (amino and bromine) groups. It is well known that conjugation shifts the absorption and emission positions to a longer wavelength. From the optical point of view, without any significant extended conjugation in compound **1**, the exhibited optical properties in the longer wavelength region are fascinating and useful for practical applications.

Our computed (under vacuum and in DCM) vertical excitation energies (VEEs) and nature transition orbitals (NTOs) for various excited electronic states of **1** indicate that the absorption maximum ( $S_0$ - $S_4$ ) and longer wavelength band ( $S_0$ - $S_1$ ) correspond to  $\pi$ ,  $\pi^*$  and  $n$ ,  $\pi^*$  transitions (Fig. S7 and S8, ESI†). The fluctuation in the electron density during these electronic transitions can be seen in the provided NTOs (Fig. 4d). Furthermore, the excitation maximum (at 530 nm) of **1** also supports the existence of the lowest excited state ( $S_1$ ) in the longer wavelength region (Fig. S6d, ESI†). The crystals of **1** exhibit a single emission peak around 590 nm after (Fig. S9a and b, ESI†) and before (Fig. S9c, ESI†) 400 nm excitation in the solid state. However, when compound **1** is excited at the absorption maximum in the solution state (Fig. S5b, ESI†), in addition to the strong emission peak in the region of 525–650 nm, a weak emission peak centred at 425 nm is observed. The intense peak is red-shifted but does not become a weak peak on increasing

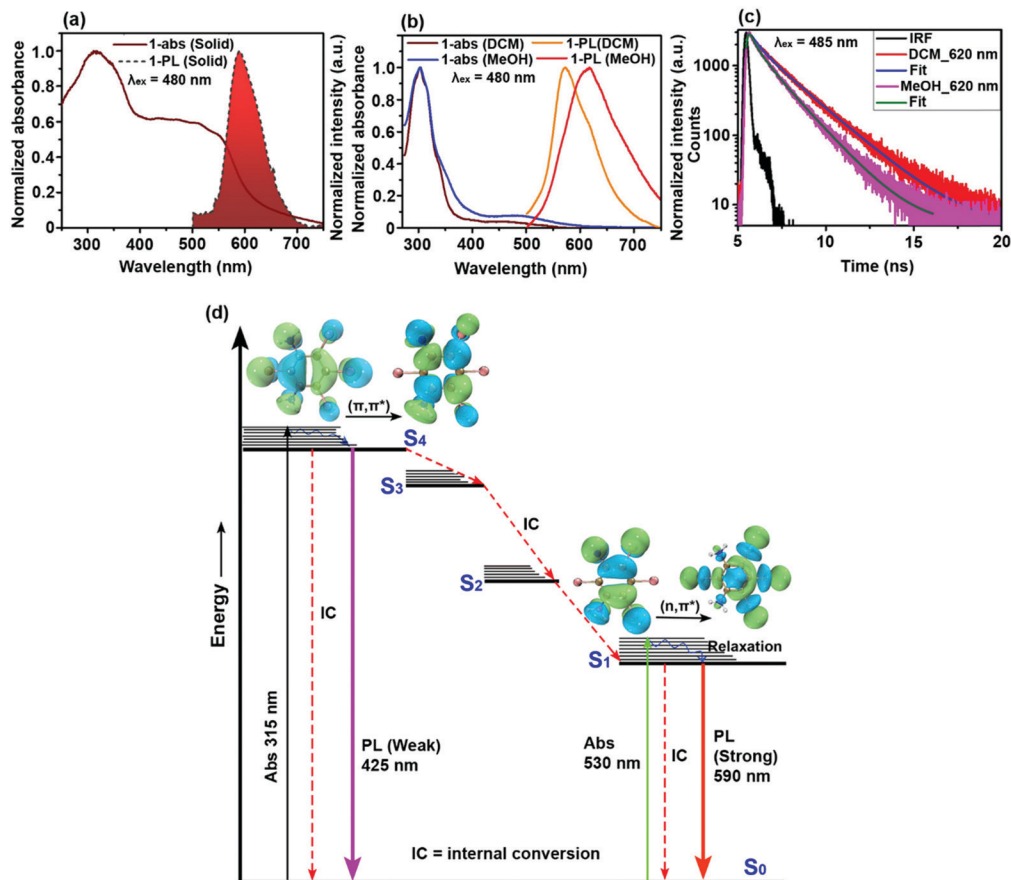


Fig. 4 Absorption and emission spectra of compound **1** in (a) solid and (b) solution. (c) The PL decay traces of **1** when monitored at 620 nm and (d) schematic representation of the plausible photo-physical processes involved in the origin of orange emission of compound **1**. The NTOs corresponding to  $S_1$  and  $S_4$  states are shown here.

the polarity of the solvent. In the absorption and PL spectra, the polarity sensitive and insensitive nature of higher and lower wavelength peaks indicate the  $n, \pi^*$  and  $\pi, \pi^*$  characters of transitions. This experimental optical behaviour of compound **1** is also supported by the computational calculations, in particular, by the nature of transitions (Fig. S7 and S8, ESI<sup>†</sup>). These observations indicate that compound **1** exhibits an orange emission from the  $S_1$  state in both solid and solution states, even after excitation to the  $S_4$  state (Fig. S5b and S9c, ESI<sup>†</sup>). This indicates the significance of the ultrafast internal conversion process prior to the emission from the  $S_1$  state (Fig. 4d).<sup>61</sup> Furthermore, the NTOs corresponding to the  $S_1$  state indicate the movement of electrons located at the amino and Br groups to the aromatic ring during electronic excitation.

It is important to note that without having significant extended conjugation in compound **1**, the developed stable  $S_1$  state in the longer wavelength region is due to the interaction of nonbonding electrons/lone pairs located at the amino and Br groups with the neighbouring molecules. These interactions reflected as a weak broad shoulder in the region of 400–600 nm of the DRS spectrum (Fig. 4a). It is evident from the SCXRD analysis (Fig. 2b) that compound **1** exhibits isotropic and weak dispersive interactions. These isotropic and weak (less than  $2 \text{ kcal mol}^{-1}$ ) dispersive or soft interactions (a type of

charge-transfer)<sup>62</sup> by  $\text{Br} \cdots \text{Br}$ ,  $\text{C}-\text{N} \cdots \text{Br}$  play a significant role in extending the absorption to a longer wavelength and hence resulted in orange emission. The relative quantum yield of compound **1** is found to be 9% from rhodamine 6G as the standard (Table S2, ESI<sup>†</sup>). The PL decay traces of compound **1** when monitored at 620 nm well fit with the single exponential equation (Fig. 4c). The fluorescence lifetime of compound **1** is found to be  $2.1 (\pm 0.01) \text{ ns}$  in DCM and  $1.7 (\pm 0.01) \text{ ns}$  in MeOH, respectively. All photo-physical parameters such as radiative and non-radiative rate constants, *etc.*, are shown in Table S2 (ESI<sup>†</sup>).

As single crystals of compound **1** exhibited interesting elastic and optical properties, their potential application in optical waveguides was investigated in both unbent and bent crystals. The details of the experimental setup and the approach of bending the crystal prior to recording the emission are shown in the ESI<sup>†</sup>. The single crystals under both conditions were excited with a pulsed laser ( $\lambda_{\text{ex}} = 532 \text{ nm}$ ) at different positions and the resulting emission was recorded at one end of the crystal (Fig. 5b and e). The propagated orange emission to one end of the crystal in unbent and bent shaped crystals can be seen in Fig. 5a and b. As observed in both the shapes of the crystal, the emission intensity at the end of the crystal gradually decreases on increasing the distance between the excited and

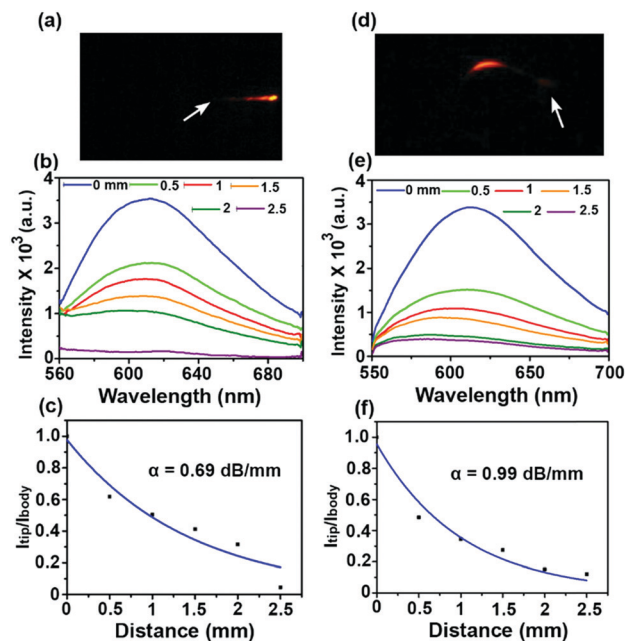


Fig. 5 Optical waveguides of the crystals of compound **1** with unbent (a–c) and bent shaped crystals (d–f). (a and d) Optical microscopy images of crystals upon excitation ( $\lambda_{\text{ex}} = 532$  nm) at one end and bent position, describing the waveguide characteristics. (b and e) Emission spectra recorded at one end of the crystal with various distances (0–2.5 mm) between the end and excitation position. (c and f) Optical loss coefficient ( $\alpha$ ) was determined when the emission decay is fitted with a single exponential function.

the end position. Furthermore, the peak maximum ( $\lambda = 610$  nm) in both the shapes is slightly red-shifted when compared with the solid state emission (Fig. 4a). Upon fitting the data, the optical loss coefficient ( $\alpha$ ) was found to be  $0.69 \text{ dB mm}^{-1}$  for unbent (Fig. 5c) and  $0.99 \text{ dB mm}^{-1}$  for bent shape (Fig. 5f) of the crystals. These  $\alpha$  values are lower or comparable to those of few organic crystals and representative polymers (Table S3, ESI<sup>†</sup>), indicating the applicability of single crystals of compound **1** in flexible optical waveguides. However, these  $\alpha$  values are higher when compared with those of a few monoaromatic fluorophores<sup>28,29</sup> and organic crystals (Table S3, ESI<sup>†</sup>). The reason might be due to the significant re-absorption effect, which can be observed because of the considerable overlap of the absorption and emission spectrum of compound **1** (Fig. 4a) in the wavelength region of 550–650 nm.

Overall, the mechanical and optical responses of single crystals of compound **1** can be summarized as follows. Fundamentally, the approach of investigating the mechanical properties (mode of external stimuli is the mechanical force) and the optical properties (mode of excitation source is photons) of crystals is different. Therefore, controlling of one property by the other and understanding its subsequent changes requires the help of multiple instrumentation techniques. However, both the properties are connected to various types of strong and weak non-covalent interaction driven molecular packings. Therefore, regulation of appropriate packing features is one of the ways of achieving both the properties. Furthermore,

intermolecular interactions can be controlled through suitable design and substitution of functional groups. In this context, our design and synthesis of compound **1** with bromine and amino functional groups helped significantly in controlling the required molecular packing features to achieve both the properties. The presence of a relatively large number of non-bonding electrons surrounding the benzenoid ring facilitates the rotation of molecules without affecting the continuity of crystal packing. Furthermore, our computed NTOs in **1** suggest the role of both amino and Br groups during excitation. The relaxed molecule to the lowest vibrational state of  $S_1$  emits the orange light in the unbent and bent shapes of crystals, which is also supported by the lack of a considerable change in the peak maxima of the emission spectra (Fig. 5b and e). These results indicate that even after the elastic bending of the crystal, there is no significant perturbation in the energy of the singlet electronic states. Thus, the observed elastic flexibility and orange emission by single crystals of **1** are linked to the isotropic and weak dispersive (soft) intermolecular interaction guided molecular packing.

## Conclusions

In summary, single crystals of a newly designed and synthesized compound **1** are found to exhibit excellent elastic flexibility and high elastic strain at room temperature under external flexural mechanical stress. The observed isotropic and weak dispersive intermolecular interaction guided molecular packing is responsible for the origin of elastic properties. The computed NTOs indicate that the  $S_1$  state has  $n, \pi^*$  character. The abundant non-bonding electrons present in compound **1** due to amino and Br groups, and their interaction with the neighbouring molecules resulted in the absorption/excitation band in the higher wavelength region. The single crystals of **1** exhibited an orange emission when excited at 530 nm. The fluorescence lifetime of compound **1** is found to be 2.1 ns. The experimentally observed optical behaviour was rationalized by the TDDFT studies. Given the advantages of both mechanical and optical properties of **1**, a flexible optical waveguide has been realized. This work demonstrates the significance of soft interactions in realizing the mechanical flexibility and practically useful optical properties of organic single crystals, which are important for the development of flexible crystalline materials for future technologies.

## Conflicts of interest

There are no conflicts to declare.

## Acknowledgements

VG and PC acknowledge IIT-Kharagpur for a post-doctoral and doctoral research fellowship. SD thanks CSIR, India, for a research fellowship. We acknowledge DST (SERB) (EMR/2017/001499), New Delhi, India, for the financial support and DST-FIST for providing the single crystal X-ray diffractometer.

We gratefully acknowledge the Centre for Theoretical Studies and Department of Chemistry, IIT-Kharagpur, for providing computational facilities. CMR thanks DST (New Delhi) for the Swarnajayanti Fellowship (DST/SJF/CSA-02/2014-15).

## References

- G. R. Desiraju, *Crystal Engineering: The Design of Organic Solids*, Elsevier, New York, 1989.
- S. Saha, M. K. Mishra, C. M. Reddy and G. R. Desiraju, *Acc. Chem. Res.*, 2018, **51**, 2957–2967.
- P. Naumov, S. Chizhik, M. K. Panda, N. K. Nath and E. Boldyreva, *Chem. Rev.*, 2015, **115**, 12440–12490.
- P. Naumov, D. P. Karothu, E. Ahmed, L. Catalano, P. Commins, J. M. Halabi, M. B. Al-Handawi and L. Li, *J. Am. Chem. Soc.*, 2020, **142**, 13256–13272.
- E. Ahmed, D. P. Karothu and P. Naumov, *Angew. Chem., Int. Ed.*, 2018, **57**, 8837–8846.
- S. Varughese, M. S. R. N. Kiran, U. Ramamurty and G. R. Desiraju, *Angew. Chem., Int. Ed.*, 2013, **52**, 2701–2712.
- X. Fang, X. Yang and D. Yan, *J. Mater. Chem. C*, 2017, **5**, 1632–1637.
- X. Yang, L. Ma and D. Yan, *Chem. Sci.*, 2019, **10**, 4567–4572.
- X. Yang, X. Lin, Y. Zhao, Y. S. Zhao and D. Yan, *Angew. Chem., Int. Ed.*, 2017, **56**, 7853–7857.
- B. Zhou and D. Yan, *Angew. Chem., Int. Ed.*, 2019, **58**, 15128–15135.
- S. Hayashi, S. Yamamoto, D. Takeuchi, Y. Ie and K. Takagi, *Angew. Chem., Int. Ed.*, 2018, **57**, 17002–17008.
- R. Huang, C. Wang, Y. Wang and H. Zhang, *Adv. Mater.*, 2018, 1800814.
- H. Liu, Z. Lu, Z. Zhang, Y. Wang and H. Zhang, *Angew. Chem., Int. Ed.*, 2018, **57**, 8448–8452.
- H. Liu, Z. Bian, Q. Cheng, L. Lan, Y. Wang and H. Zhang, *Chem. Sci.*, 2019, **10**, 227–232.
- J. M. Halabi, E. Ahmed, L. Catalano, D. P. Karothu, R. Rezgoui and P. Naumov, *J. Am. Chem. Soc.*, 2019, **141**, 14966–14970.
- B. Liu, H. Liu, H. Zhang, Q. Di and H. Zhang, *J. Phys. Chem. Lett.*, 2020, **11**, 9178–9183.
- L. Catalano, D. P. Karothu, S. Schramm, E. Ahmed, R. Rezgoui, T. J. Barber, A. Famulari and P. Naumov, *Angew. Chem., Int. Ed.*, 2018, **57**, 17254–17258.
- S. Chen, H. Yin, J. Wu, H. Lin and X. D. Wang, *Sci. China Mater.*, 2020, **63**, 1613–1630.
- M. Annadhasan, A. R. Agrawal, S. Bhunia, V. V. Pradeep, S. S. Zade, C. M. Reddy and R. Chandrasekar, *Angew. Chem., Int. Ed.*, 2020, **59**, 13852–13858.
- M. Annadhasan, D. P. Karothu, R. Chinnasamy, L. Catalano, E. Ahmed, S. Ghosh, P. Naumov and R. Chandrasekar, *Angew. Chem., Int. Ed.*, 2020, **59**, 2–12.
- M. Annadhasan, S. Basak, N. Chandrasekhar and R. Chandrasekar, *Adv. Opt. Mater.*, 2020, **8**, 2000959.
- Y. L. Shi and X. D. Wang, *Adv. Funct. Mater.*, 2021, **31**, 2008149.
- M. P. Zhuo, G. P. He, Y. Yuan, Y. C. Tao, G. Q. Wei, X. D. Wang, S. T. Lee and L. S. Liao, *CCS Chem.*, 2020, **2**, 413–424.
- G. M. Krishna, R. Devarapalli, G. Lal and C. M. Reddy, *J. Am. Chem. Soc.*, 2016, **138**, 13561–13567.
- S. Ghosh and C. M. Reddy, *Angew. Chem., Int. Ed.*, 2012, **51**, 10319–10323.
- A. Worthy, A. Grosjean, M. C. Pfrunder, Y. Xu, C. Yan, G. Edwards, J. K. Clegg and J. C. McMurtrie, *Nat. Chem.*, 2018, **10**, 65–69.
- S. Dey, S. Das, S. Bhunia, R. Chowdhury, A. Mondal, B. Bhattacharya, R. Devarapalli, N. Yasuda, T. Moriwaki, K. Mandal, G. D. Mukherjee and C. M. Reddy, *Nat. Commun.*, 2019, **10**, 3711.
- B. Liu, Q. Di, W. Liu, C. Wang, Y. Wang and H. Zhang, *J. Phys. Chem. Lett.*, 2019, **10**, 1437–1442.
- B. Liu, Z. Lu, B. Tang, H. Liu, H. Liu, Z. Zhang, K. Ye and H. Zhang, *Angew. Chem., Int. Ed.*, 2020, **59**, 23117–23121.
- K. Yadava, X. Qin, X. Liu and J. J. Vittal, *Chem. Commun.*, 2019, **55**, 14749–14752.
- C. M. Reddy, K. A. Padmanabhan and G. R. Desiraju, *Cryst. Growth Des.*, 2006, **6**, 2720–2731.
- C. M. Reddy, M. T. Kirchner, R. C. Gundakaram, K. A. Padmanabhan and G. R. Desiraju, *Chem. – Eur. J.*, 2006, **12**, 2222–2234.
- C. M. Reddy, R. C. Gundakaram, S. Basavoju, M. T. Kirchner, K. A. Padmanabhan and G. R. Desiraju, *Chem. Commun.*, 2005, 3945–3947.
- M. Shimizu, Y. Takeda, M. Higashi and T. Hiyama, *Angew. Chem., Int. Ed.*, 2009, **48**, 3653–3656.
- B. Tang, C. Wang, Y. Wang and H. Zhang, *Angew. Chem., Int. Ed.*, 2017, **56**, 12543–12547.
- R. Huang, B. Liu, C. Wang, Y. Wang and H. Zhang, *J. Phys. Chem. C*, 2018, **122**, 10510–10518.
- T. Beppu, K. Tomiguchi, A. Masuhara, Y. J. Pu and H. Katagiri, *Angew. Chem., Int. Ed.*, 2015, **54**, 7332–7335.
- B. Tang, H. Liu, F. Li, Y. Wang and H. Zhang, *Chem. Commun.*, 2016, **52**, 6577–6580.
- E. Cho, J. Choi, S. Jo, D. H. Park, Y. K. Hong, D. Kim and T. S. Lee, *ChemPlusChem*, 2019, **84**, 1130–1134.
- M. Shimizu, *Chem. Rec.*, 2021, **21**, 1–18.
- H. Liu, S. Yan, R. Huang, Z. Gao, G. Wang, L. Ding and Y. Fang, *Chem. – Eur. J.*, 2019, **25**, 16732–16739.
- Z. Xiang, Z. Y. Wang, T. B. Ren, W. Xu, Y. P. Liu, X. X. Zhang, P. Wu, L. Yuan and X. B. Zhang, *Chem. Commun.*, 2019, **55**, 11462–11465.
- J. Kim, J. H. Oh and D. Kim, *Org. Biomol. Chem.*, 2021, **19**, 933–946.
- R. Zhou, Y. Cui, J. Dai, C. Wang, X. Liang, X. Yan, F. Liu, X. Liu, P. Sun, H. Zhang, Y. Wang and G. Lu, *Adv. Opt. Mater.*, 2020, **8**, 1902123.
- J. M. Gere and B. J. Goodno, *Mechanics of Materials*, Cengage Learning, Stanford, CT, 8th edn, 2013.
- M. K. Mishra and C. C. Sun, *Cryst. Growth Des.*, 2020, **20**, 4764–4769.

- 47 S. Hayashi and T. Koizumi, *Chem. – Eur. J.*, 2018, **24**, 8507–8512.
- 48 T. Lu and F. Chen, *J. Comput. Chem.*, 2012, **33**, 580–592.
- 49 V. Gude and K. Biradha, *J. Phys. Chem. C*, 2021, **125**, 120–129.
- 50 S. Saha and G. R. Desiraju, *Chem. Commun.*, 2018, **54**, 6348–6351.
- 51 V. Gude, M. Karmakar, A. Dey, P. K. Datta and K. Biradha, *Phys. Chem. Chem. Phys.*, 2020, **22**, 4731–4740.
- 52 S. Ghosh, M. K. Mishra, S. B. Kadambi, U. Ramamurty and G. R. Desiraju, *Angew. Chem., Int. Ed.*, 2015, **54**, 2674–2678.
- 53 M. K. Mishra, K. Mishra, S. A. S. Asif and P. Manimunda, *Chem. Commun.*, 2017, **53**, 13035–13038.
- 54 R. Devarapalli, S. B. Kadambi, C. T. Chen, R. K. Gamidi, B. R. Kammari, M. J. Buehler, U. Ramamurty and C. M. Reddy, *Chem. Mater.*, 2019, **31**, 1391–1402.
- 55 M. K. Mishra, S. B. Kadambi, U. Ramamurty and S. Ghosh, *Chem. Commun.*, 2018, **54**, 9047–9050.
- 56 J. P. Perdew, K. Burke and M. Ernzerhof, *Phys. Rev. Lett.*, 1996, **77**, 3865–3868.
- 57 N. Godbout, D. R. Salahub, J. Andzelm and E. Wimmer, *Can. J. Chem.*, 1992, **70**, 560–571.
- 58 C. Sosa, B. Andzelm, C. Elkin, E. Wimmer, K. D. Dobbs and D. A. Dixon, *J. Phys. Chem.*, 1992, **96**, 6630–6636.
- 59 R. E. Stratmann and G. E. Scuseria, *J. Chem. Phys.*, 1998, **109**, 8218–8224.
- 60 M. J. Frisch, G. W. Trucks, H. B. Schlegel, G. E. Scuseria, M. A. Robb, J. R. Cheeseman, G. Scalmani, V. Barone, B. Mennucci, G. A. Petersson, H. Nakatsuji, M. Caricato, X. Li, H. P. Hratchian, A. F. Izmaylov, J. Bloino, G. Zheng, J. L. Sonnenberg, M. Hada, M. Ehara, K. Toyota, R. Fukuda, J. Hasegawa, M. Ishida, T. Nakajima, Y. Honda, O. Kitao, H. Nakai, T. Vreven, J. A. Montgomery Jr., J. E. Peralta, F. Ogliaro, M. Bearpark, J. J. Heyd, E. Brothers, K. N. Kudin, V. N. Staroverov, T. Keith, R. Kobayashi, J. Normand, K. Raghavachari, A. Rendell, J. C. Burant, S. S. Iyengar, J. Tomasi, M. Cossi, N. Rega, J. M. Millam, M. Klene, J. E. Knox, J. B. Cross, V. Bakken, C. Adamo, J. Jaramillo, R. Gomperts, R. E. Stratmann, O. Yazyev, A. J. Austin, R. Cammi, C. Pomelli, J. W. Ochterski, R. L. Martin, K. Morokuma, V. G. Zakrzewski, G. A. Voth, P. Salvador, J. J. Dannenberg, S. Dapprich, A. D. Daniels, O. Farkas, J. B. Foresman, J. V. Ortiz, J. Cioslowski and D. J. Fox, *Gaussian 09, Revision A.1*, Gaussian, Inc., Wallingford, CT, 2009.
- 61 M. Pollum and C. E. Crespo-Hernandez, *J. Chem. Phys.*, 2014, **140**, 071101.
- 62 L. P. Wolters, P. Schyman, M. J. Pavan, W. L. Jorgensen, F. M. Bickelhaupt and S. Kozuch, *Wiley Interdiscip. Rev.: Comput. Mol. Sci.*, 2014, **4**, 523–540.